Chemical Science

EDGE ARTICLE

View Article Online
View Journal | View Issue

Two roaming pathways in the photolysis of CH_3CHO between 328 and 308 nm†

Kin Long K. Lee,‡[a] Mitchell S. Quinn,‡[a] Alan T. Maccarone,§[b] Klaas Nauta,[a] Paul L. Houston,[c] Scott A. Reid,¶[b] Meredith J. T. Jordan[b] and Scott H. Kable*[a]

Cite this: Chem. Sci., 2014, 5, 4633

Received 29th July 2014
Accepted 22nd August 2014

DOI: 10.1039/c4sc02266a

www.rsc.org/chemicalscience

The correlated speed and rotational energy distributions of the CO fragment from photodissociation of CH_3CHO have been measured at a range of wavelengths from 308 to 328 nm. The distributions are bimodal, showing low J, slow speed, and high J, fast speed components. The cold component disappears for $\lambda > 325$ nm. This threshold corresponds to C–H bond cleavage and we assign these CO products as arising from roaming of a H-atom about a CH_3CO core. We attribute the hot component to CO formed through CH_3-roaming. No evidence was observed for the presence of a transition state mechanism. This is the first time two distinct roaming channels have been observed from the same electronic state. The results support the growing understanding that roaming can be significant in chemical reactions and outweigh traditional pathways.

Introduction

The near-ultraviolet (UV) photochemistry of acetaldehyde, CH_3CHO, has been studied for many decades. It is an important atmospheric trace species and its spectroscopy and photochemistry are considered to be typical of carbonyl species in general. Before 2006, the near-ultraviolet photochemistry of CH_3CHO was considered to comprise three photochemical pathways:[1]

$$CH_3CHO + h\nu \rightarrow CH_3CHO(S_1) \xrightarrow{\text{ISC to } T_1} CH_3 + HCO \quad (E^* = 375.4) \tag{1}$$

$$CH_3CHO + h\nu \rightarrow CH_3CHO(S_1) \xrightarrow{\text{IC to } S_0} CH_4 + CO, \ \textit{via}\ \text{TS} \quad (E^* = 346.9) \tag{2}$$

$$CH_3CHO + h\nu \rightarrow CH_3CHO(S_1) \xrightarrow{\text{IC to } S_0} CH_3CO + H \quad (E^* = 367.4) \tag{3}$$

where ISC, IC and TS are abbreviations for intersystem crossing, internal conversion and transition state, respectively. The threshold energy in kJ mol^{-1} for each pathway, E^*, is indicated. Energies were adopted from the ESI of ref. 2, from original sources.[3–5] These pathways are shown schematically as (1) to (3) in Fig. 1.

In less than a decade, our knowledge of CH_3CHO photochemistry has changed markedly. In 2006, a roaming pathway, producing CH_4 + CO, labeled (4) below and in Fig. 1, was reported.[6]

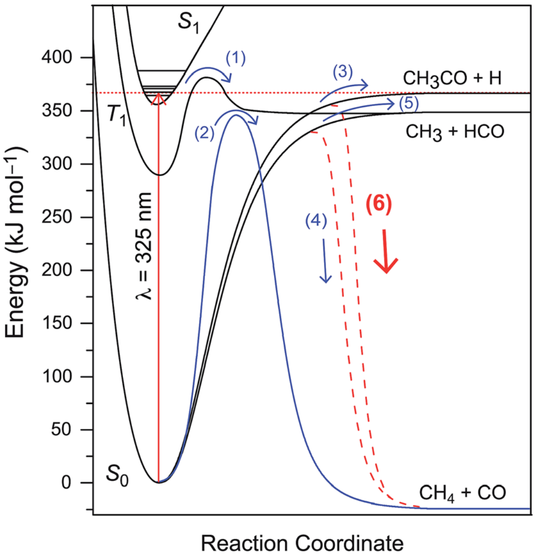

Fig. 1 Schematic of the potential energy surface of CH_3CHO showing 6 different photochemical pathways. The numbers on each pathway refer to the numbered chemical equations in the text.

---

[a] School of Chemistry, University of New South Wales, Kensington, NSW, 2052, Australia. E-mail: s.kable@unsw.edu.au

[b] School of Chemistry, University of Sydney, Sydney, NSW 2006, Australia

[c] School of Chemistry and Biochemistry, Georgia Institute of Technology, Atlanta, GA, 30332, USA

† Electronic supplementary information (ESI) available: A more complete description of experimental details and the complete set of experimental data. See DOI: 10.1039/c4sc02266a

‡ These authors contributed equally to this work and should be considered joint first authors.

§ Present address: Department of Chemistry, University of Wollongong, NSW, 2522, Australia.

¶ Present address: Department of Chemistry, Marquette University, Milwaukee, WI, 53201, USA.

$$CH_3CHO + h\nu \rightarrow CH_3CHO(S_1) \xrightarrow{\text{IC to } S_0} CH_4 + CO, \quad \textit{via}\text{ roaming} \quad (E^* \leq 346.9) \tag{4}$$

Roaming can be thought of as an effectively barrierless self-reaction (an "intra-molecular abstraction") occurring between incipient bond dissociation products late in the bond dissociation product channel.[7–9] In (4), this is CH_3 abstracting the formyl H atom to form CH_4 + CO.[10]

A further three pathways or mechanisms have been reported since 2006. An S_0 pathway, (5), with the same products as (1), was reported in 2009.[11] This is important to the present discussion because all roaming pathways have an associated, barrierless, bond cleavage pathway, and it is perhaps unusual that the roaming pathway was discovered before the simple bond cleavage pathway on the S_0 surface.

$$CH_3CHO + h\nu \rightarrow CH_3CHO(S_1) \xrightarrow{\text{IC to } S_0} CH_3 + HCO \quad (E^* = 346.9) \tag{5}$$

Two further pathways are important in CH_3CHO photolysis. Triple fragmentation to H + CO + CH_3,[12–14] has an energetic threshold that lies slightly above the photolysis energies used here[12] (the threshold energy corresponds to $\lambda_{\text{photolysis}} = 288$ nm). Phototautomerisation to CH_2CHOH (ref. 15–17) has been discovered recently for photolysis wavelengths in the range used here, but this process requires collisional stabilization, which is not present in the molecular beam environment of this work. The competition between roaming and transition state (TS) pathways, (2) and (4), is the subject of this paper.

Roaming was first conclusively demonstrated as a new class of reaction mechanisms in 2004, when detailed quasiclassical trajectory (QCT) simulations were used to interpret velocity map ion imaging experiments describing the photodissociation of formaldehyde, H_2CO.[7] Here, translational energy distributions of the H_2 + CO products were experimentally determined for defined CO rotational states. The two distinct, *J*-dependent, distributions were then interpreted, with the aid of the QCT simulations, as arising from a standard, TS, mechanism, the major channel, and a second, minor channel, the roaming mechanism. In this case a H atom abstracted a second H from the incipient HCO radical to form H_2 + CO.[7–9]

Houston and Kable (HK) subsequently proposed a roaming mechanism in a second system, CH_3CHO, based on the existence of correlated bimodal rotational and translational distributions in the CO product arising from 308 nm photolysis of CH_3CHO.[6] Similar to the earlier studies on H_2CO, QCT simulations of 308 nm photolysis were then performed on a high quality, global, full dimensional potential energy surface (PES) for CH_3CHO.[18,19] These QCT simulations supported the existence of a roaming pathway and predicted roaming to be the dominant mechanism for formation of CH_4 + CO.[19] Since these first two examples of roaming were identified, roaming has been found or predicted in a wide variety of systems.[8,20–32]

The initial experiments of HK enabled the relative importance of the roaming and TS channels to be estimated. By integrating the two components of the CO rotational distribution they attributed 15% of the CH_4 + CO flux to be due to roaming, (4), and 85% to the TS pathway, (2). Heazlewood *et al.*, in a joint experimental/theoretical paper, subsequently measured the CH_4 internal energy.[10] By comparison with QCTs on a global, full dimensional CH_3CHO PES, they inferred the reverse branching ratio: 84% roaming and 16% TS. These authors also reported evidence in the QCT calculations of a second roaming pathway. The dominant pathway involved a CH_3 group roaming about the HCO core, while the minor pathway involved a H atom roaming about a CH_3CO core. However, a clear signature for each could not be discerned and this observation was not quantified. In 2012, Rubio-Lago *et al.* (RL) measured the kinetic energy release in the CO fragment[33] and reported the roaming branching to be ~20% at 308 nm.

This discrepancy in branching between roaming and TS pathways is important; if roaming is a minor component then conventional transition state theory will predict the rate coefficient for CH_4 + CO production to within ~15%. However, if roaming is dominant, conventional kinetic theories will fail. Although Harding *et al.* have located "roaming transition states",[20] these involve large amplitude, anharmonic motion, and trajectories show multiple re-crossing of the roaming TS. As such, these roaming TS's cannot currently be used in standard reaction rate theories. There have been two attempts to develop a statistical theory of roaming with the objective of producing a broadly applicable kinetic theory. The theory of Klippenstein and co-workers[34] relies on accurate descriptions of the potential energy surface, which means that this theory is not readily transferable to other molecules. Andrews *et al.* have developed a very simple statistical theory for the branching fraction of roaming and radical reactions, which, when combined with other kinetic theories, could yield rate coefficients for roaming reactions.[35] However, this theory has only been compared to limited experimental data. Thus, resolving the existing discrepancy about the importance of roaming in CH_3CHO may provide a major impetus to the development of new kinetic theories of roaming.

Here, we investigate the photolysis of CH_3CHO at a range of energies, from 308 nm, to lower energy, approaching and crossing the threshold for CH_3CO + H formation, reaction (3). The data provide experimental evidence and branching ratios for two roaming pathways and in doing so reconcile all previous experiments. The presence of two roaming mechanisms has implications for all photochemical and thermal unimolecular reactions as discussed below.

Experimental

Experiments were performed with a velocity map imaging apparatus described previously.[36] CH_3CHO, in a molecular beam of He, was photolysed with a laser at $\lambda = 308$–328 nm. CO fragments were probed by (2 + 1) resonance-enhanced multiphoton ionization (REMPI) spectroscopy *via* the B–X band system. Due to a small amount of one-laser background signal from the probe laser at ~230 nm, all images were recorded by alternately toggling the pump laser on/off for 100 shots at a time. Total accumulation for the images was typically 50 000 laser shots at 10 Hz. Ions were individually centroided and counted.[37]

Acetaldehyde is well known to polymerize in the liquid state and we found that it clusters readily in a supersonic expansion. Photolysis of CH_3CHO clusters produces cold CO that interferes with detection of CO from the monomer. The extensive lengths taken to eliminate clusters are described in ESI.†

Two-dimensional (2D) REMPI-ion images were collected at 308 nm. This technique is a hybrid of the Doppler-free method reported by Suits and co-workers[38] and the 3D REMPI-ion imaging reported by Dick and co-workers.[39] In this technique a software mask is applied to the detector to record only ions that fly perpendicular to the laser propagation axis. This provides Doppler-free spectral resolution.[38] A 1D array is recorded for each laser wavelength. The laser is stepped and the process repeated, building up a representation of the ion image as a function of laser wavelength. The intensity of each pixel is multiplied by distance from the center of the image to account for the smaller detection efficiency of faster moving fragments. This correction is only valid for isotropic distributions. Full CO images were collected at many pump and probe laser wavelengths to confirm that the CO was isotropic in all cases. We also checked that the CO speed distribution was the same when measured from ion images, and when reconstructed from the 2D-REMPI ion images. A full description of the experiment is available in ESI.†

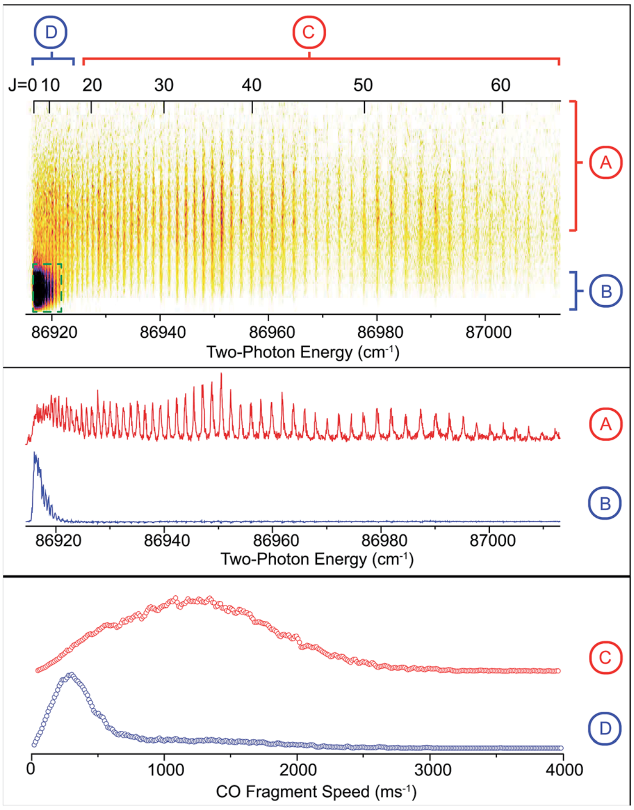

Fig. 2 (top) 2D-REMPI-ion image of the CO fragments from 308 nm photolysis of CH_3CHO; (centre) REMPI spectra from the 2D image by integrating the two regions indicated; (bottom) speed distribution obtained by integrating the indicated regions.

Results

308 nm images

A 2D-REMPI-ion image scan is shown in Fig. 2. Laser wavenumber is plotted on the horizontal axis while CO recoil speed is plotted vertically. Each horizontal slice is a (2 + 1) REMPI spectrum of CO for molecules with a specific speed. The rotationally resolved spectrum corresponds to the 0–0 band of the B–X system of CO. The structure consists of a dense Q-branch, spreading with individually resolved rotational transitions to higher wavenumber.[38] A comb of J values is indicated in the figure. The spectra labeled (A) and (B) were obtained by integrating the image over the indicated regions. At low speed (B), the spectrum consists almost solely of low-J peaks, while the spectrum at high speed (A) shows CO produced with a wide range of J. Each vertical stripe in the image is the speed distribution at specific J(CO). The distributions are independent of J for $J \geq 15$. For $J < 15$, however, there is an intense component at low speed. The 2D image has been integrated for $J \geq 15$, (C) and $J < 15$, (D) to produce the speed distributions plotted below the image.

The image in Fig. 2 shows convincingly that there are two, and only two, clearly different distributions of energy in the CO fragment from the 308 nm photolysis of CH_3CHO. The two components are sufficiently distinguished in 2D space that it is reasonable to integrate them directly to obtain branching fractions. If the box in the figure defines the cold component, then the ratio of this integrated intensity to the whole total intensity is 13 ± 3%, where the error represents sensible choices of boundary.

Full ion images at 308 nm photolysis were measured at a variety of J. Two of these, at $J = 7/8$ (the peaks are not fully resolved in our experiment) and $J = 30$ are shown in Fig. 3. These values of J were chosen with reference to Fig. 2 as representative of the distinct hot and cold components in the distribution. The high-J speed distribution is fit well by a single Boltzmann distribution with $T(\text{rot}) = 2700 \pm 300$ K, drawn through the data as a red line. The low-J speed distribution can be fit to two Boltzmann components, a low temperature component with $T(\text{rot}) = 340 \pm 30$ K and a high temperature component with $T(\text{rot}) = 2700 \pm 300$ K, shown as blue and red lines, respectively. The errors quoted represent variations in fitting repeated ion images measured at a variety of J values. The 2700 K speed component appears to be independent of J, as shown in Fig. 2 and as evidenced from analysis of ion images obtained at a number of different J values.

Energy dependent images

The absorption cross section of acetaldehyde becomes rapidly smaller for $\lambda > 308$ nm,[40] which caused the signal from the CO fragment to also reduce, causing the 2D-REMPI ion images to be very noisy. Nonetheless, accumulation for 50 000 laser shots still resulted in good quality ion images. The excitation

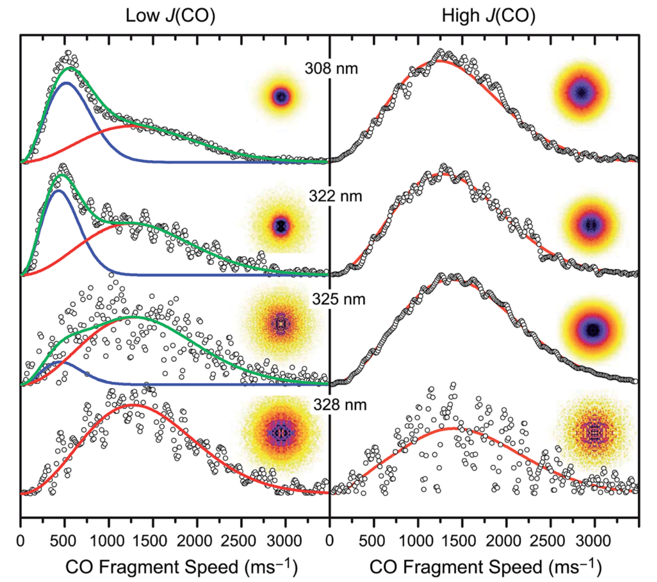

Fig. 3 CO speed distributions and two Boltzmann fits to the data (see Table 1). The cold component in the low-J data disappears for photolysis between 325 and 328 nm.

Table 1 Boltzmann fitting parameters for the two speed distributions at $J = 7/8$, shown in Fig. 3

λ (nm) (vac)	$\tilde{\nu}$ (cm^{-1}) (vac)	Fraction "Cold" (%)	"Hot" T (K)	"Cold" T (K)
308.44	32 421	48 ± 3	2700 ± 300	340 ± 30
315.07	31 739	43 ± 3	2290 ± 300	340 ± 30
320.44	31 207	46 ± 3	2550 ± 300	340 ± 30
322.44	31 014	37 ± 3	2650 ± 300	310 ± 30
325.33	30 738	11 ± 5	2780 ± 300	300 ± 100
328.13	30 476	0 ± 3	2730 ± 500	—

spectrum of CH_3CHO below the triplet threshold ($\lambda_{\text{photolysis}} >$ 318.5 nm)[41] is very structured[11] so photolysis wavelengths were optimized for CO signal. Full ion images were obtained at a variety of J for 5 photolysis wavelengths between 328 and 315 nm. Fig. 3 shows images and speed distributions at three wavelengths (others are shown in ESI†), at the same CO J values reported for 308 nm: $J = 7/8$ and $J = 30$. The speed distributions at $J = 30$ show no dependence on the photolysis wavelength. All are fit by Boltzmann distributions in the range 2290–2780 K (Table 1 and red lines in Fig. 3). At low J the speed distributions clearly contain two components. The high-speed components were fit by the same Boltzmann function as at high J (red lines); Fig. 2 demonstrates that this is part of the same overall hot distribution extending into this J range. The cold components (blue lines) were fit by a Boltzmann distribution with $T = 300$–340 K (Table 1).

The most striking aspect in the low-J speed distributions is that the cold component diminishes with decreasing photolysis energy. The cold fraction of the distribution at $J = 7/8$, determined by integrating the blue Boltzmann functions in Fig. 3, is reported in Table 1. It is constant, within the fitting error, as photolysis energy is lowered from 308 nm to 320 nm then drops sharply until it is no longer discernible at 328 nm.

Discussion

Comparison with previous work at 308 nm

The 2D-REMPI ion image in Fig. 2 covers the complete CO ($\nu = 0$) product distribution and shows two components, implying two discernable mechanisms. These two CO rotational and speed distributions have been observed previously in CH_3CHO photolysis at 308 nm. Assuming two Gaussian functions to fit the rotational distribution, HK estimated 15% cold fraction.[6] Assuming two Boltzmann speed distributions, RL determined 20% cold fraction.[33] Our measurement of 13 ± 3% for the cold fraction is in qualitative agreement with both previous values, but does not require any assumption governing the shape of the distributions.

Single temperature fits of the CO Doppler widths obtained by HK yield an average CO translational energy of 43 kJ mol^{-1} at $J = 46$, and 12 kJ mol^{-1} at $J = 1$.[6] In comparison, average CO translational energies of 34 ± 4 kJ mol^{-1} at $J = 30$, and 3.4 ± 0.4 kJ mol^{-1} at $J = 7/8$ were obtained from our velocity map ion images. The high J results are consistent and our ion images indicate a single temperature fit is appropriate at high J. The variation at low J is readily explained. It is clear from Fig. 2 and 3 that there are two components to the low J speed distributions and the previous single temperature fit yields an average over these distributions.[6] Although no translational energies or temperatures were reported by RL, the speed distribution we obtain at $J = 30$, is consistent with the shape of their $J = 50$ translational energy distribution.[33]

Energy dependence

The two clearly distinguished energy distributions are evidence that the CO fragments arise from different mechanisms. The disappearance of the cold component between 325 and 328 nm indicates an energy threshold. The threshold for CH_3CO + H is 367.4 kJ mol^{-1}, corresponding to a photon of 325.6 nm.[4] The correspondence between the disappearance of the cold component and the energetic threshold for C–H bond breaking is strongly reminiscent of H-atom roaming in H_2CO,[7] which has a threshold that lies 87–205 cm^{-1} below that for CH-bond cleavage.[42] We therefore conclude that the cold component corresponds to roaming of a H atom about a CH_3CO core. This attribution is consistent with the predictions of Heazlewood *et al.* based on QCT simulations on a global CH_3CHO PES.[10] The H-roaming pathway is shown energetically as pathway (6) in Fig. 1 and as a cartoon in the table of contents graphic.

Assignment of the cold component of the CO distribution to H-roaming leads us naturally to query the origin of the hot component. The literature describes two other mechanisms for CH_4 + CO production – the TS and CH_3-roaming mechanisms.[6,10,33] The question is which should be assigned to the hot component? Bowman and co-workers reported QCT calculations for photolysis of CH_3CHO at this energy.[10,18,19] The CO rotational distribution for the TS mechanism produced a highly inverted population with a maximum near $J = 60$, while the CH_3-roaming mechanism produced a distribution that was broadly similar to the distribution HK[6] reported.[19] Similarly, the measured CH_4 internal energy distribution was poorly described by QCT calculations of the TS mechanism.[10] We therefore attribute the hot component of the CO distribution to be (mostly) CH_3-roaming, (4).

We now combine our conclusions with the previous results to arrive at a single consistent picture of CH_3CHO photolysis, starting at 308 nm where the data are extensive. The data of HK, RL and this work all demonstrate two components to the CO rotational and translational distributions with a cold fraction of 13 ± 3% (this work), 15% (HK) and 20% (RL). Given the different techniques, we consider these to be in good agreement. The results here identify this mechanism as H-roaming, whereas previously it was assigned to CH_3-roaming. HK and RL assigned the hot component to the TS mechanism, but our results, in comparison with Heazlewood[10] and other theory,[18,19] identify this component as CH_3-roaming.

The TS mechanism, if it is present, either produces much faster, or higher angular momentum CO than measured in any experiment, which we consider unlikely, or is obscured beneath one of the other components. The only experimental evidence for presence of the TS mechanism is the vector correlation data of HK.[6] A correlation between the velocity and angular momentum vectors was observed at very high J, which was absent at lower J.[6] Theory indicates that the TS mechanism should produce such a correlation, but that CH_3-roaming should not.[18] Therefore, it seems that CO distributions arising from the TS mechanism must lie under the very high-J tails of our hot component rotational distributions, but are not experimentally discernible in the speed or rotational distributions. The only estimate of the TS fraction arises from the QCTs: 16 ± 10%.[10] Combining all the experimental and theoretical evidence, we determine the branching fraction between the three pathways for CH_4 + CO at 308 nm to be: CH_3-roaming (reaction (4)): 71 ± 12%; H-roaming (6): 13 ± 3%; and TS (2): 16 ± 10%. These branching fractions are consistent with all previous work.

Conclusions

We have measured correlated CO rotational and translational distributions from the photolysis of CH_3CHO and a variety of wavelengths between 328 and 308 nm, revealing the presence of two components in the CO energy distribution. At lower photolysis energy the cold component disappears. The close correspondence of this threshold with the threshold for CH_3CO + H, and the strong similarity with roaming data for H_2CO, leads us to conclude that the cold component arises from the roaming of a H atom about a CH_3CO core. Comparison with theory, and previous data, then leads us to conclude that the high-energy component is dominated by CH_3 roaming.

Significantly, roaming produces more stable products at the expense of more reactive products – typically molecules at the expense of radicals – and thus has consequences to atmospheric and combustion modeling. Although there is a growing consensus that roaming mechanisms are nearly universal,[7,43] and roaming has been previously observed in two different electronic states,[31] this is the first time that two distinct roaming channels have been observed from the same electronic state. Roaming has also been inferred in the thermal dissociation of CH_3CHO.[44] The natural extension of our observation here is that roaming pathways are likely to be associated with all barrierless, bond-cleavage processes in all electronic states, irrespective of whether they are the lowest energy pathway, in all photochemical and thermal unimolecular reactions.

Acknowledgements

This work was supported by the Australian Research Council (grant number DP130104326).

Notes and references

1 R. Atkinson, *et al.*, *Atmos. Chem. Phys.*, 2006, **6**, 3625–4055.

2 B. R. Heazlewood, A. T. Maccarone, D. U. Andrews, D. L. Osborn, L. B. Harding, S. J. Klippenstein, M. J. T. Jordan and S. H. Kable, *Nat. Chem.*, 2011, **3**, 443–448.

3 B. J. Smith, M. T. Nguyen, W. J. Bouma and L. Radom, *J. Am. Chem. Soc.*, 1991, **113**, 6452–6458.

4 B. Ruscic, *et al.*, *J. Phys. Chem. Ref. Data*, 2005, **34**, 573–656.

5 L. B. Harding, Y. Georgievskii and S. J. Klippenstein, *J. Phys. Chem. A*, 2010, **114**, 765–777.

6 P. L. Houston and S. H. Kable, *Proc. Natl. Acad. Sci. U. S. A.*, 2006, **103**, 16079–16082.

7 D. Townsend, S. A. Lahankar, S. K. Lee, S. D. Chambreau, A. G. Suits, X. Zhang, J. Rheinecker, L. B. Harding and J. M. Bowman, *Science*, 2004, **306**, 1158–1161.

8 J. M. Bowman and B. C. Shepler, *Annu. Rev. Phys. Chem.*, 2011, **62**, 531–553.

9 A. G. Suits, *Acc. Chem. Res.*, 2008, **41**, 873.

10 B. R. Heazlewood, M. J. T. Jordan, S. H. Kable, T. M. Selby, D. L. Osborn, B. C. Shepler, B. J. Braams and J. M. Bowman, *Proc. Natl. Acad. Sci. U. S. A.*, 2008, **105**, 12719–12724.

11 B. R. Heazlewood, S. J. Rowling, A. T. Maccarone, M. J. T. Jordan and S. H. Kable, *J. Chem. Phys.*, 2009, **130**, 054310.

12 G. de Wit, B. R. Heazlewood, M. S. Quinn, A. T. Maccarone, K. Nauta, S. A. Reid, M. J. T. Jordan and S. H. Kable, *Faraday Discuss.*, 2012, **157**, 227–241.

13 K.-C. Hung, P.-Y. Tsai, H.-K. Li and K.-C. Lin, *J. Chem. Phys.*, 2014, **140**, 064313.

14 P. Morajkar, A. Bossolasco, C. Schoemaecker and C. Fittschen, *J. Chem. Phys.*, 2014, **140**, 21408.

15 G. da Silva, *Angew. Chem., Int. Ed.*, 2010, **49**, 7523–7525.

16 D. U. Andrews, B. R. Heazlewood, A. T. Maccarone, T. Conroy, R. J. Payne, M. J. T. Jordan and S. H. Kable, *Science*, 2013, **337**, 1203–1206.

17 A. E. Clubb, M. J. T. Jordan, S. H. Kable and D. L. Osborn, *J. Phys. Chem. Lett.*, 2012, **3**, 3522–3526.

18 B. C. Shepler, B. J. Braams and J. M. Bowman, *J. Phys. Chem. A*, 2007, **111**, 8282–8285.

19 B. C. Shepler, B. J. Braams and J. M. Bowman, *J. Phys. Chem. A*, 2008, **112**, 9344–9351.

20 L. B. Harding, S. J. Klippenstein and A. W. Jasper, *Phys. Chem. Chem. Phys.*, 2007, **9**, 4055–4070.

21 V. Goncharov, N. Herath and A. G. Suits, *J. Phys. Chem. A*, 2008, **112**, 9423–9428.

22 M. H. Chao, P. Y. Tsai and K. C. Lin, *Phys. Chem. Chem. Phys.*, 2011, **13**, 7154–7161.

23 M. L. Hause, N. Herath, R. Zhu, M. C. Lin and A. G. Suits, *Nat. Chem.*, 2011, **3**, 932–937.

24 R. Sivaramakrishnan, M. C. Su, J. V. Michael, S. J. Klippenstein, L. B. Harding and B. Ruscic, *J. Phys. Chem. A*, 2011, **115**, 3366–3379.

25 L. B. Harding and S. J. Klippenstein, *J. Phys. Chem. Lett.*, 2010, **1**, 3016–3020.

26 M. P. Grubb, M. L. Warter, A. G. Suits and S. W. North, *J. Phys. Chem. Lett.*, 2010, **1**, 2455–2458.

27 M. P. Grubb, M. L. Warter, K. M. Johnson and S. W. North, *J. Phys. Chem. A*, 2011, **115**, 3218–3226.

28 E. Kamarchik, L. Koziol, H. Reisler, J. M. Bowman and A. I. Krylov, *J. Phys. Chem. Lett.*, 2010, **1**, 3058–3065.

29 R. S. Zhu and M. C. Lin, *Chem. Phys. Lett.*, 2009, **478**, 11–16.

30 H. Xiao, S. Maeda and K. Morokuma, *J. Phys. Chem. Lett.*, 2011, **2**, 934–938.

31 M. P. Grubb, M. L. Warter, H. Xiao, S. Maeda, K. Morokuma and S. W. North, *Science*, 2012, **335**, 1075–1078.

32 M. P. Grubb, M. L. Warter and S. W. North, *Phys. Chem. Chem. Phys.*, 2012, **14**, 6733–6740.

33 L. Rubio-Lago, G. A. Amaral, A. Arregui, J. González-Vázquezac and L. Bañares, *Phys. Chem. Chem. Phys.*, 2012, **14**, 6067–6078.

34 S. J. Klippenstein, Y. Georgievskii and L. B. Harding, *J. Phys. Chem. A*, 2011, **115**, 14370–14381.

35 D. U. Andrews, S. H. Kable and M. J. T. Jordan, *J. Phys. Chem. A*, 2013, **117**, 7631–7642.

36 N. Hobday, M. S. Quinn, K. Nauta, D. U. Andrews, M. J. T. Jordan and S. H. Kable, *J. Phys. Chem. A*, 2013, **117**, 12091–12103.

37 W. Li, D. Chambreau, S. A. Lahankar and A. G. Suits, *Rev. Sci. Instrum.*, 2005, **76**, 063106.

38 V. Goncharov, H. Nuradhika, A. Arregui, L. Bañares and A. G. Suits, *J. Phys. Chem. A*, 2009, **113**, 3840–3843.

39 A. Schmaunz, U. Kensy, A. Slenczka and B. Dick, *Phys. Chem. Chem. Phys.*, 2009, **11**, 7115–7119.

40 G. K. Moortgat, H. Meyrehn and P. Warneck, *ChemPhysChem*, 2010, **11**, 3896.

41 G. A. Amaral, A. Arregui, L. Rubio-Lago, J. D. Rodriguez and L. Bañares, *J. Chem. Phys.*, 2010, **133**, 064303.

42 S. A. Lahankar, V. Goncharov, F. Suits, J. Farnum, J. M. Bowman and A. G. Suits, *Chem. Phys.*, 2008, **347**, 288–299.

43 N. Herath and A. G. Suits, *J. Phys. Chem. Lett.*, 2011, **2**, 642–647.

44 R. Sivaramakrishnan, J. V. Michael and S. J. Klippenstein, *J. Phys. Chem. A*, 2010, **114**, 755–764.